Ordered Porous Carbons with Tunable Pore Sizes as Catalyst Supports in Direct Methanol Fuel Cell

Geun Seok Chai,[†] Suk Bon Yoon,[†] Jong-Sung Yu,*[,†] Jong-Ho Choi,[‡] and Yung-Eun Sung[‡]

Department of Chemistry, Hannam University, Daejeon, 306-791, Republic of Korea, and School of Chemical Engineering, Seoul National University, Seoul 151-744, Republic of Korea

Received: October 9, 2003; In Final Form: March 18, 2004

Ordered uniform porous carbon frameworks with pore sizes in the range of 10 to ~1000 nm were synthesized against removable colloidal silica crystalline templates by carbonization of phenol and formaldehyde as a carbon precursor. The porous carbons were used as supports for a Pt(50)−Ru(50) alloy catalyst to study their supporting effect on the anodic performance of the catalyst in a direct methanol fuel cell (DMFC). The use of the ordered uniform porous carbons resulted in much improved catalytic activity for methanol oxidation in the fuel cell probably due to their high surface areas, large pore volumes, and three-dimensionally interconnected uniform pore structures, which allow a higher degree of dispersion of the catalysts and efficient diffusion of reagents. In general, the smaller the pore sizes in the porous carbons were, the better the catalytic activity for methanol oxidation was. In addition, as pore sizes are getting smaller, the structural integrity with good pore interconnection seems to be getting more important for the catalytic oxidation of methanol. Among the porous carbons studied in this work, the one with about 25 nm in pore diameter (PtRu−C-25) showed the highest performance with power densities of ~58 and ~167 mW/cm^2 at 30 and 70 °C, respectively. These values roughly correspond to ~70 and ~40% increase as compared to those of a commercially available Pt−Ru alloy catalyst (E-TEK), respectively.

Introduction

Porous materials with three-dimensionally (3-D) interconnected ordered structures are technologically important for a variety of applications including the use as catalysts, supports, separation systems, sensors, adsorbents, electronic materials, double-layer capacitors, and hydrogen storage materials.[1,2] Recently, a remarkable progress has been made in the synthesis of carbons with periodic porous structures. This progress was achieved by a replication method using templates, such as zeolites,[3] ordered mesoporous silicas,[4,5] and silica colloidal crystals[6,7] for the synthesis of ordered microporous (pore size <2 nm), mesoporous (2−50 nm), and macroporous (>50 nm) carbons, respectively. In these cases, the porous carbons were fabricated through carbonization of polymers preformed in the void spaces of the inorganic porous templates and subsequent removal of the templates. Colloidal crystalline templates based on spherical silica nanoparticles have been applied for the synthesis of uniform mesoporous and macroporous carbon materials.[6−8] Recently, the fabrication of new ordered uniform porous carbons with spherical cavities of 50 to ~70 nm in diameter interconnected to each other was reported by carbonization of sugars and polymers.[9,10] The carbon capsules with hollow spherical core and mesoporous shell structures were also synthesized using silica spheres with solid core and mesoporous shell structures as templates.[11]

The direct methanol fuel cell (DMFC) has recently attracted great attention for its future potential as a clean and ideal power source. To increase the catalytic activity of methanol electrooxidation, intense studies have been devoted mainly toward the development of new catalysts such as binary,[12] ternary,[13] and even quaternary[14] metal catalysts. These catalysts are generally dispersed as small particles on conductive supports such as a carbon black with a high surface area to give the high dispersion of the catalysts.[15] Recently, in addition to the development of catalysts themselves, there also arises a great attention for new carbon materials as supports to help achieve optimum catalytic performance. High surface area and well-developed porosity are essential for a catalyst support to result in high catalytic activity.[16] Carbon black, called Vulcan XC-72 (a registered trade name from CABOT), has been commonly used as a carbon support for electrode catalysts in DMFCs. Vulcan XC-72 carbon consists of an aggregation of amorphous carbon nanoparticles with sizes in the range of 30 to ~60 nm. In fact, commercially available E-TEK catalysts are Pt−Ru alloys supported on the Vulcan XC-72. Recently, several different carbon materials such as mesostructured carbon materials,[17] graphitic carbon nanofibers,[18] and mesocarbon microbeads[19] were reported as supports of Pt or Pt alloy catalysts mainly for higher dispersion of the catalysts and for improved synergistic effects. In our earlier work, highly ordered uniform porous carbon frameworks with a spherical cavity of ~200 nm in diameter were synthesized against removable colloidal silica crystalline templates.[20] The Pt(50)−Ru(50) catalyst supported by these ordered uniform porous carbons resulted in about a 10 to ~15% increase in methanol oxidation activity as compared to that of the corresponding commercially available Pt−Ru alloy catalyst. This demonstrated their potential as catalyst supports for methanol oxidation in a fuel cell. One of the advantages of the colloidal crystalline template method is that the pore sizes of the carbon

* To whom correspondence should be addressed. Phone: (+82) 42-629-7446. Fax: (+82) 42-629-7469. E-mail: jsyu@mail.hannam.ac.kr.
[†] Hannam University.
[‡] Seoul National University.

10.1021/jp0370472 CCC: $27.50
Published on Web 04/30/2004

SCHEME 1: Synthetic Procedure for Uniform Porous Carbons of Tunable Pore Sizes through Colloidal Crystal Template Approach

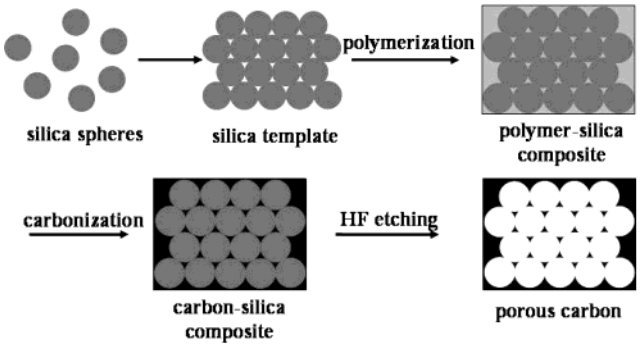

structure can be easily controlled in the range of several nanometers to several micrometers by varying the silica spheres in the colloidal crystal template. Such pore size control can render porous carbons with regulated surface area, pore volume, and structural integrity. But, it is challenging to synthesize smaller silica spheres with uniform sizes, especially as the particle sizes are becoming smaller than 50 nm in diameter. Here, we extend the synthesis of uniform porous carbon replicas with different pore sizes through the colloidal crystal templates of silica spheres of 15 to ~1000 nm in diameter by carbonization of cross-linked phenol and formaldehyde as a carbon precursor. To investigate the support effect, the Pt(50)−Ru(50) alloy catalysts were prepared by borohydride reduction using the porous carbons as catalyst supports. The use of the porous carbons as supports significantly increased catalytic activity for methanol oxidation in the fuel cell as compared to that of the commercially available Pt−Ru catalyst.

Experimental Procedures

Preparation of Silica Spheres, Porous Carbons, and Pt−Ru Catalysts. Several monodisperse silica nanoparticles in the range of 15 to ~1000 nm were synthesized using a modification of the procedure described by Osseo-Asare et al.[21a] and Stober et al.[21b] Uniform porous carbon replica was synthesized against a colloidal crystal template by polymerization of phenol and formaldehyde as a carbon precursor followed by subsequent carbonization according to the reported methods.[4,10,20] The overall synthetic procedure of the ordered porous carbon is described in Scheme 1. The resulting ordered porous carbons were termed C−X, where X indicates the pore size of the carbons.

The Pt(50)−Ru(50) catalysts were prepared by a borohydride reduction method.[22] Equal moles (2×10^{-3} mol) of $H_2PtCl_6 \cdot 6H_2O$ and $RuCl_3 \cdot xH_2O$ were dissolved in 250 mL of water, and then the solution was diluted to make a metal salt solution with a total metal concentration of ~2.0 mM and stirred at ambient temperature for 1 h. The pH of the solution was adjusted to pH = ~8 with dropwise addition of 20 wt % NaOH solution. The required amount of a carbon substrate (porous carbon or Vulcan XC-72) was suspended in deionized water and stirred to form a homogeneous carbon slurry. Then, the metal salt solution was added into the carbon slurry. The metal loading was 60 wt % for the Vulcan XC-72 like in the commercially available E-TEK catalyst and 80 wt % for the porous carbons. Since the porous carbons have high surface areas, it was possible to have a higher metal loading of 80 wt % as well as the same metal loading of 60 wt %. This also gives an extra benefit that the amount of carbon support used can be decreased to half. The $NaBH_4$ solution was prepared by dissolving 1.5 g of $NaBH_4$ (0.04 mol) in 40 mL of water, and the entire volume was quickly poured into the metal salt solution. The Pt−Ru/C reaction mixture was stirred for 2 h. Pt−Ru/C was collected at the bottom of the flask overnight. The catalyst was filtered, rinsed thoroughly several times with deionized water, and dried in a vacuum oven at 80 °C. The resulting supported catalysts were named PtRu−C−X. The Rt−Ru catalyst prepared on the Vulcan XC-72 carbon black support was named PtRu−VC.

Characterization. The nitrogen adsorption and desorption isotherms were measured at −196 °C using a Micromeritics ASAP 2010 system. Specific surface areas of the porous carbons were determined by nitrogen adsorption data in the relative pressure range from 0.05 to 0.2 using the BET (Brunauer−Emmett−Teller) equation. Total pore volumes were estimated from the amount of nitrogen adsorbed at a relative pressure of 0.987. Micropore volumes of the porous carbons were also calculated from the analysis of the adsorption isotherms using the Horvath−Kawzoe method.[23] Pore-size distribution curves were obtained from the analysis of the adsorption branches of the nitrogen isotherms using the BJH (Barrett−Joyner−Halenda) method.

X-ray diffraction (XRD) patterns of the supported catalysts were obtained with a Rigaku diffractometer with CuKα radiation at a scan rate of 4°/min. The X-ray source was operated at 40 kV and 30 mA. Powder samples were mounted on glass slides. Surface morphologies of the porous carbons were examined by a scanning electron microscope (SEM, LEO 1455VP, Hitach S-4700) operated at an acceleration voltage of 25 kV. The microscopic features of the sample were observed with a transmission electron microscope (TEM, EM 912 Omega) operated at 200 kV.

Electrochemical Measurements. Cyclic voltammetric measurements were carried out in a three-electrode cell with Ag/AgCl (in saturated KCl) as a reference electrode and platinum gauge as a counter electrode. The reference electrode contacted an electrolyte solution via a Luggin capillary. The working electrode was prepared by painting a small amount of the supported catalyst slurry on a Teflonized carbon paper (TGPH-090) and drying in an oven at 120 °C for 1 h under Ar gas. The effective geometric area of the electrode was 1 cm^2, and the electrode had a catalyst loading (metal base) of 2.0 mg/cm^2. All cyclic voltammograms were obtained at room temperature at a scan rate of 20 mV/s in a mixed solution of 0.5 M H_2SO_4 and 1.0 M methanol from −0.35 to +1.35 V versus Ag/AgCl using an EG&G 362 potentiostat. The baseline curve was obtained at the same condition without the CH_3OH solution. The electrolyte solutions were purged with nitrogen gas before use for 1 h. All chemicals used were of analytical grade.

Cell performance was evaluated using a DMFC unit cell with a 2 cm^2 cross-sectional catalyst zone and measured with a potentiometer (WMPG-1000), which can record cell potentials from the circuit voltage under constant current conditions. The MEA (membrane electrode assembly) was made by hot-pressing (110 °C, 800 psi, 3 min) a pretreated Nafion117 (Du-Pont) with anode and cathode catalysts on each side. The anode consisted of a carbon paper and carbon-supported catalyst layer. The cathode consisted of a carbon paper and unsupported Pt catalyst layer from Johnson Matthey. The catalyst loadings at anode and cathode based on metal only were 3.0 and 5.0 mg/cm^2, respectively. The Nafion117 membrane was pretreated by boiling in 3 wt % H_2O_2 for 1 h and then in 0.5 M H_2SO_4 for 1 h. The single cell test fixture was composed of two copper end plates and two graphite plates with rib-channel patterns allowing

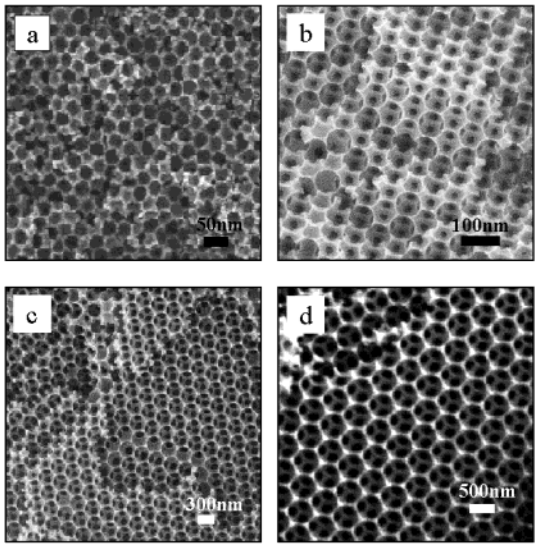

Figure 1. SEM images of (a) C-25, (b) C-68, (c) C-245, and (d) C-512.

the passage of methanol to the anode and oxygen gas to the cathode. A 2.0 M methanol solution was supplied to the anode at a rate of 1.0 mL/min by a Masterflex liquid micropump, while dry O_2 was fed to the cathode at a rate of 500 mL/min by a flowmeter.

Results and Discussion

Electron Microscopic Analysis. Figure 1 shows SEM images of the resulting porous carbon replicas with 25, 68, 245, and 512 nm in pore diameter, respectively. The pores are uniform, close-packed and roughly spherical, resulting in the formation of a highly ordered nanoporous carbon framework. Each of the spherical pores is also three-dimensionally interconnected to neighboring pores through small holes, which were generated at the contact points between silica spheres close-packed in colloidal crystal templates. Such highly ordered structures were predominantly observed for the porous carbons with relatively large pore sizes of 50 nm and higher since ordered colloidal crystalline arrays were well-prepared with the large silica spheres. However, it is challenging to synthesize uniform silica spheres with diameters less than 50 nm. The size uniformity usually decreased in such smaller size ranges. This also greatly decreased the uniformity of the colloidal crystalline arrays and eventually of the resulting porous carbon replicas. The 25 nm porous carbon showed quite some decrease in structural order but still largely maintained an overall structural integrity (Figure 1a). In the case of the 10 nm porous carbon, the structural order was greatly impaired. Overall structural integrity was significantly decreased with a nearly structural collapse probably because the wall separating the pores became too thin to support the rigidity of the overall ordered porous structure.

Figure 2 shows TEM images of the porous carbons after catalyst loading. The structural integrity was still pretty well reserved even after catalyst loading. TEM images also show homogeneous dispersion of small, spherical, and uniform dark spots that correspond to Pt−Ru alloy nanoparticles. Small agglomerates of the metal particles were also sporadically observed in the supported catalysts. The particle sizes measured directly from TEM photographs at randomly selected regions for each sample were approximately 2 to ~3 nm.

Sorption Analysis. Figure 3 shows N_2 adsorption and desorption isotherms at −196 °C for C-25 and C-68 and the corresponding carbons with Pt−Ru catalyst loaded on them.

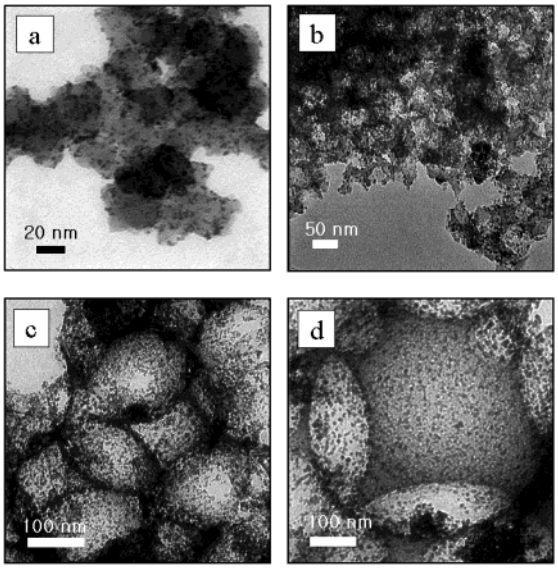

Figure 2. TEM images of carbon supported catalysts. (a) E-TEK, (b) PtRu−C-68, (c) PtRu−C-245, and (d) PtRu−C-512. Small dots shown in the figures correspond to the Pt−Ru alloy catalysts prepared on the carbon supports.

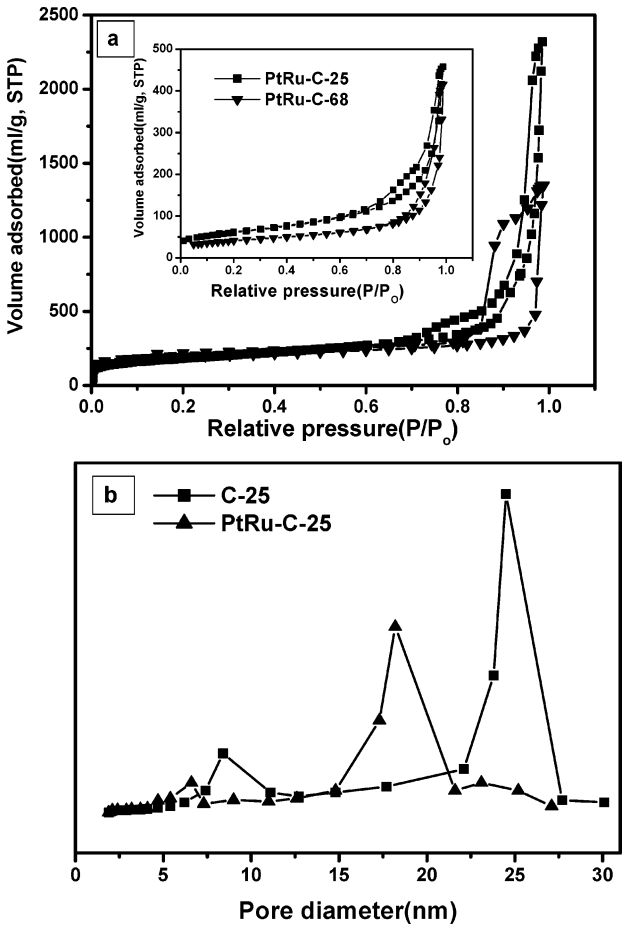

Figure 3. (a) N_2 adsorption−desorption isotherms of porous carbons, C-25 (■) and C-68 (▼). The inset shows N_2 isotherms of corresponding loaded carbons, PtRu−C-25 and PtRu−C-68. (b) Pore size distribution curves of C-25 before and after catalyst loading.

The ordered porous carbons exhibited type IV isotherms with a H1 adsorption−desorption hysteresis loop according to the IUPAC nomenclature, which are typically attributed to the adsorption in mesopores. The ordered porous carbons exhibited

TABLE 1: Structural Parameters of Porous Carbons and the Corresponding Carbons with Pt(50)−Ru(50) Catalysts Loading Prepared in This Paper

sample[a]	S_{BET} (m^2/g)	S_{micro} (m^2/g)	$S_{meso/macro}$ (m^2/g)	V_{totoal} (cc/g)	V_{micro} (cc/g)
E-TEK	93	18	75	0.19	0.01
VC	232	87	145	0.32	0.04
PtRu−VC	107	29	78	0.17	0.01
C-10	996	252	744	3.81	0.12
PtRu−C-10	159	13	146	0.55	0.01
C-25	845	304	541	3.66	0.17
PtRu−C-25	213	32	181	0.51	0.01
C-68	691	433	258	1.63	0.18
PtRu−C-68	166	46	120	0.33	0.02
C-245	605	400	205	0.81	0.16
PtRu−C-245	130	20	110	0.24	0.01
C-512	509	313	196	0.75	0.16
PtRu−C-512	118	24	94	0.22	0.02
C-806	449	267	182	0.71	0.15
PtRu−C-806	108	19	89	0.19	0.01

[a] VC indicates a Vulcan XC-72 carbon. C−X and PtRu−C−X, where C and X represent an ordered porous carbon and a pore diameter, respectively. S_{BET}: BET surface area; S_{micro}: micropore area; $S_{meso/macro}$: meso and macropore area; V_{totoal}: total pore volume; and V_{micro}: micropore volume.

a sharp capillary condensation step centered at high relative pressures (P/P_o = 0.9 to ~1.0). The capillary evaporation took place at much lower relative pressures, which indicates that connections between the pores are much narrower than the pores themselves.[10a] In the case of porous carbons with pore diameters larger than 70 nm, type II isotherms were observed characteristic of macroporous materials. The values for BET surface areas and pore volumes of the porous carbons and the corresponding loaded carbons are summarized in Table 1. In general, the smaller the pore sizes in the porous carbons were, the higher surface areas and larger pore volumes were. All the porous carbons showed higher surface areas and pore volumes than the Vulcan carbon. It is interesting to notice that the pore volumes of C-10 and C-25 were exceptionally high as compared with those of the other carbons. Adsorption on mesoporous solids proceeds via multilayer adsorption followed by capillary condensation.[24] Therefore, the capillary condensation in the mesopores is likely to contribute to the observed high steep rise at higher pressures, which resulted in a high increase in pore volume. Nitrogen condensation in the sample tube might also give such a high increase in pore volume. But about the same results were obtained for the porous carbons with such small pore sizes. Thus, the nitrogen condensation in the sample tube is unlikely. Such high pore volumes of 3.0 or higher were also reported for similar mesoporous materials in the literature.[25] Further study will be needed to address this phenomenon.

The porous carbons have not only meso-/macropores, which are templated by colloidal silica array, but also significant micropores, which are inevitably generated during the carbonization of polymer structures. C-25 showed a pore-size distribution centered around 25 nm, while it revealed the maximum peak position shifted to about 18 nm after catalyst loading (PtRu−C-25). Thus, such pore-size decrease is attributed to the loading of the nanosized metal particle on the pore surface. On the basis of the observed sorption intensities, both the surface area and the pore volume were drastically decreased after the catalyst loading as compared to those of the corresponding unloaded carbons. Particularly, the decrease of micropores was significant after the catalyst loading. The micropores decreased to one-sixth through to one-twentieth, while the meso-/macropores decreased to somewhere between half and one-quarter

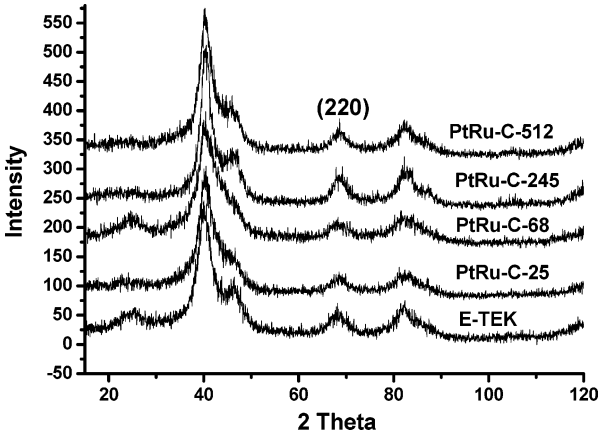

Figure 4. X-ray diffraction patterns of supported $Pt_{50}Ru_{50}$ alloy catalysts.

of those of the corresponding unloaded porous carbons, respectively, in terms of the surface areas. This strongly indicates that the catalysts may be mainly distributed in the micropore areas as evidenced from the more significant decrease of the micropores upon the catalyst loading. Thus, such a decrease in the structural parameters before and after catalyst loading is considered mainly due to covering or filling of both the micropores and the meso-/macropores in the carbons. The decrease in the structural parameters related to the possible structural degradation during the preparation of the loaded carbons in harsh synthetic conditions might be also significant in particular for C-10 and C-25 since they have rather thin walls, although carbon frameworks in general have a strong mechanical stability.[4a] Figure 2 shows TEM images of the porous carbons with relatively large pore sizes after catalyst loading. Structural integrity was still pretty well reserved even after catalyst loading. Thus, the possible structural degradation is also probable but is likely to be less significant for the large pore carbons. The minimum surface area that a support material needs to support metal particles was calculated using an equation suggested in the literature[26] and found out to be 109 m^2 for 1.0 g carbon support to disperse the PtRu catalyst particles perfectly on the support material. BET surface areas of 450 to ~1000 m^2/g determined for the porous carbons were four times or higher than the minimum surface area. But, it is difficult to distinguish both contributions related to the catalyst loading and the structural degradation quantitatively.

X-ray Analysis. The X-ray diffraction patterns of the carbon-supported catalysts are shown in Figure 4. Pure Pt has a face-centered cubic (fcc) lattice structure, while pure Ru has a hexagonal close-packed (hcp) structure. All the supported Pt−Ru catalysts exhibit XRD patterns typical of the fcc structure. No evidence of peaks related to tetragonal RuO_2 and hcp Ru phase was found in the XRD patterns, which indicates a strong evidence for the presence of the Pt−Ru catalyst as an alloy. The average particle sizes were about 2−3 nm as calculated using a Debye−Scherrer equation from the broadening of the (2.2.0) reflection in the Pt fcc lattice.[27] The size of the supported alloy nanoparticles was also investigated by TEM in Figure 2. The measured values were in good agreement with values determined from the XRD data.

Cyclic Voltammetric Analysis and Single Cell Test. Figure 5 shows cyclic voltammograms for methanol oxidation activities of PtRu−C-25, PtRu−C-68, and PtRu−VC in comparison to that of the E-TEK Pt(50)−Ru(50). The values of onset voltage that corresponds to a starting point of methanol oxidation for each catalyst were −0.01, 0.01, 0.09, and 0.07 V (vs Ag/AgCl)

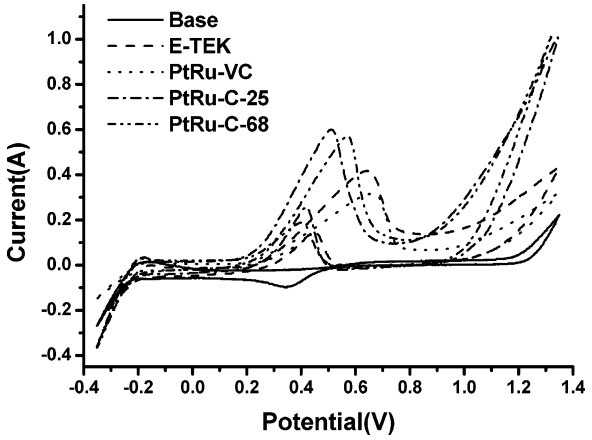

Figure 5. Cyclic voltammograms for supported $Pt_{50}Ru_{50}$ alloy catalysts.

for the PtRu−C-25, PtRu−C-68, PtRu−VC, and E-TEK catalyst, respectively. This indicates that the porous carbon-supported catalysts start the methanol oxidation on the lower voltages than the E-TEK and carbon black-supported catalysts. In addition, PtRu−C-25 and PtRu−C-68 exhibited higher methanol oxidation activities of 297 and 236 mA/mgcm^2 at 0.5 V (vs Ag/AgCl), respectively, as compared to 141 mA/mgcm^2 for the E-TEK catalyst and 104 mA/mgcm^2 for the PtRu−VC catalyst. This corresponds to a better performance of the porous carbon supported catalysts over the E-TEK one by about 60 to ∼106%. Interestingly, the PtRu−VC catalyst prepared in the same condition as the porous carbon-supported catalysts showed lower oxidation activity as well as higher onset voltage than those of the E-TEK catalyst also supported on the Vulcan carbon. This may indicate that the Pt−Ru alloy catalyst itself prepared in this work is inferior to the E-TEK catalyst in terms of methanol oxidation activity since the same Vulcan XC-72 carbon was used as a support for both cases. Even then, the Pt−Ru catalysts prepared on the porous carbons showed much better performance than that of the E-TEK catalyst. Thus, such an increase in activity may be attributed solely to the supporting effect of the porous carbon.

Figure 6 shows the unit cell performance of direct methanol fuel cell at 30 and 70 °C by the porous carbon-supported catalysts as compared to those of the PtRu−VC and E-TEK catalysts. The catalyst loadings were 3.0 mg/cm^2 (metal loading base) for each of the supported Pt−Ru anode catalysts and 5.0 mg/cm^2 for Pt black (Johnson Matthey) cathode catalyst, respectively. At 30 °C (Figure 6a), the open-circuit voltages (OCV) were 0.646, 0.672, 0.662, 0.654, and 0.651 V for E-TEK, PtRu−C-25, PtRu−C-68, PtRu−C-245, and PtRu−C-512, respectively. The maximum power densities were 33, 58, 46, 42, and 39 mW/cm^2, respectively. This indicates that the porous carbon-supported catalysts exhibited 15−75% higher power density than the E-TEK catalyst. Similar trends were also observed at 70 °C as shown in Figure 6b. The OCV values were found to be 0.694, 0.715, 0.723, 0.714, 0.709, 0.706, and 0.703 V for E-TEK, PtRu−C-10, PtRu−C-25, PtRu−C-68, PtRu−C-245, PtRu−C-512, and PtRu−C-806, respectively. The maximum power densities were 117, 152, 167, 145, 138, 129, and 122 mW/cm^2, respectively. All the porous carbon supported Pt−Ru catalysts exhibited much higher specific activity for methanol oxidation than the E-TEK catalyst and PtRu−VC catalyst by about 5−43% and 10−50%, respectively. Also, the supported catalysts showed reproducible consistent stable catalytic activities for 5 days. In general, the smaller the pore sizes in the porous carbons were, the higher the surface areas

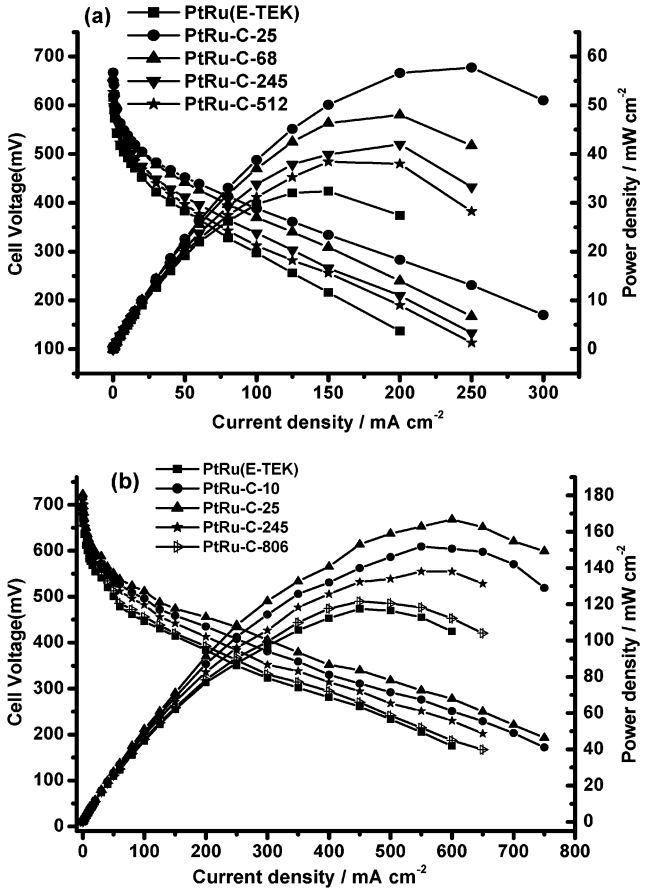

Figure 6. Voltage and power density responses of porous carbon supported $Pt_{50}Ru_{50}$ alloy catalysts as compared to that of E-TEK catalyst in direct methanol fuel cell. The DMFCs were operated (a) at 30 °C and (b) at 70 °C. Anode: supported Pt−Ru alloy catalyst (3.0 mg/cm^2). Cathode: Johnson Matthey Pt black (5.0 mg/cm^2).

and the better catalytic activities were. The general trend of the catalytic activity was in good accordance with that of the cyclic voltammograms. On the basis of the observed sorption and activity data, the improved activity for the methanol oxidation is considered to be due to the higher surface areas and larger pore volumes that the porous carbon can provide for the higher degree of catalyst dispersion. The porous carbon with a 10 nm pore diameter had the highest surface area and pore volume studied in this work. PtRu−C-10 showed very high activity for methanol oxidation but was found to give a little less activity than that of PtRu−C-25. As silica particles are getting smaller, it is becoming more difficult to synthesize them uniformly. Thus, it is also more difficult to prepare ordered porous carbon replicas with uniform pores from them. The carbon walls, particularly in the case of the porous carbons with very small pore size, may become too thin to maintain an integrated porous framework, resulting in the collapse of porous structures, which could lower the support effect. Therefore, in addition to the high surface area and pore volume, the structural integrity with the pore interconnectivity also seems to play an important role in the performance of the catalyst support. In fact, the three-dimensionally interconnected pore system in the porous carbon as a diffusion layer can favor efficient fuel and product diffusion as compared to that of the Vulcan carbon, which has randomly distributed pores of varying sizes and thus make fuel and product diffusion difficult. After all, the uniform ordered porous carbons have a high surface area and pore volume and well-integrated interconnected pore structures with tunable pore diameters,

which can allow a much wider dispersion of active catalysts and efficient diffusion of reagents, thus significantly improving the catalytic activity. Also, the preparation method was very simple with the use of relatively cheap chemicals and can be easily applied for a scaled-up process.

Conclusions

The colloidal silica template presented in this paper was a simple and viable route for the production of ordered porous carbons with high surface areas and large pore volumes, whose pore sizes can be easily controlled by monitoring the sizes of the silica spheres. Thus, the replication method enables the preparation of porous carbons with a broad range of structural properties. The porous carbon supported Pt−Ru alloy catalysts exhibited a much higher catalytic activity for methanol oxidation than those of carbon black supported counterparts. This is considered to be not only due to the higher surface areas and larger pore volumes, which allow higher degree of catalyst dispersion, but also due to highly integrated interconnected pore systems with periodic order, which allow efficient gas diffusion. In general, the smaller the pore sizes in the porous carbons were, the higher the surface areas, the larger the pore volumes, and the better the catalytic activities were. In this work, the porous carbon with a 25 nm pore diameter (PtRu−C-25) demonstrated the highest performance with a power density of 167 mW/cm^2 at 70 °C, which corresponds to a 43% increase as compared to that of a commercially available catalyst.

Acknowledgment. Authors thank KOSEF (R01-2001-00424) for its financial support and the Korean Basic Science Institute in Deajeon and Jeonju for TEM and SEM analyses.

References and Notes

(1) (a) Marsh, H.; Heintz, E. A.; Rodriguez-Reinoso, F. *Introduction to Carbon Technology*; Universidad de Alicante, Secretariado de Publications: Alicante, Spain, 1997. (b) Marsh, H.; Heintz, E. A.; Rodriguez-Reinoso, F. *Sciences of Carbon Materials*; Universidad de Alicante, Secretariado de Publications: Alicante, Spain, 2000. (c) Patrick, J. W. *Porosity in Carbons: Characterization and Applications*; Edward Arnold: London, 1995. (d) Kinoshita, K. *Carbon: Electrochemical and Physicochemical Properties*; Wiley: New York, 1988. (e) Marsh, H. *Introduction to Carbon Science*; Butterworths: London, 1989.

(2) (a) Frackowiak, E.; Beguin, F. *Carbon* **2001**, *39*, 937. (b) Lillo-Rodenas, M. A.; Carratala, J.; Cazorla-Amoros, D.; Linares-Solano, A. *Fuel Processing Technology* **2002**, *77*, 331. (c) Lillo-Rodenas, M. A.; Lozano-Castello, D.; Cazorla-Amoros, D.; Linares-Solano, A. *Carbon* **2001**, *39*, 751.

(3) (a) Ma, Z.; Kyotani, T.; Tomita, A. *Chem. Commun*. **2000**, 2365. (b) Johnson, S. A.; Brigham, E. S.; Ollivier, P. J.; Mallouk, T. E. *Chem. Mater*. **1997**, *9*, 2448.

(4) (a) Yoon, S. B.; Kim, J. Y.; Yu, J.-S. *Chem. Commun*. **2002**, 1536. (b) Yoon, S. B.; Kim, J. Y.; Yu, J.-S. *Chem. Commun*. **2001**, 559. (c) Kim, J. Y.; Yoon, S. B.; Kooli, F.; Yu, J.-S. *J. Mater. Chem*. **2001**, *11*, 2912. (d) Yoon, S. B.; Kim, J. Y.; Yu, J.-S. *Chem. Mater*. **2003**, *15*, 1932. (e) Vix-Cuterl, C.; Boulard, S.; Parmentier, J.; Werckmann, J.; Patarin, J. *Chem. Lett*. **2002**, 1062.

(5) (a) Yoon, S. B.; Kim, J. Y.; Kooli, F.; Lee, C. W.; Yu, J.-S. *Chem. Commun*. **2003**, 1740. (b) Vinu, A.; Streb, C.; Murugesan, V.; Hartman, M. *J. Phys. Chem. B* **2003**, *107*, 8297. (c) Yu, C.; Fan, J.; Tian, B.; Zaho, D. Stucky, G. D. *Adv. Mater*. **2002**, *14*, 1742. (d) Kim, S. S.; Lee, D.-G.; Shah, J.; Pinnavaia, T. J. *Chem. Commun*. **2003**, 1436. (e) Kruk, M.; Jaroniec, M.; Kim, T.-W,; Ryoo, R. *Chem. Mater*. **2003**, *15*, 2815.

(6) Zakhidov, A. A.; Baughman, R. H.; Iqbal, Z.; Cui, C.; Khayrullin, I.; Dantas, S. O.; Marti, J.; Ralchenko, V. G. *Science* **1998**, *282*, 897.

(7) Li, Z.; Jaroniec, M. *J. Am. Chem. Soc*. **2001**, *123*, 9208.

(8) Han, S.; Hyeon, T. *Chem. Commun*. **1999**, 1955.

(9) (a) Yu, J.-S.; Yoon, S. B.; Chai, G. S. *Carbon* **2001**, *39*, 1421. (b) Gundiah, G.; Govindaraj, A.; Rao, C. N. R. *Mater. Res. Bull.* **2001**, *36*, 1751. (c) Lei, Z.; Zhang, Y.; Wang, H.; Ke, Y.; Li, J.; Li, F.; Xing, J. *J. Mater. Chem*. **2001**, *11*, 1975.

(10) (a) Kang, S. K.; Yu, J.-S.; Kruk, M.; Jaroniec, M. *Chem. Commun*. **2002**, 1670. (b) Yu, J.-S.; Lee, S. J.; Yoon, S. B. *Mol. Cryst. Liq. Cryst.* **2001**, *371*, 107. (c) Sung, I. K.; Yoon, S. B.; Yu, J.-S.; Kim, D. P. *Chem. Commun.* **2002**, 1480. (d) Kim, J. C.; Kim, Y. N.; Chi, E. O.; Hur, N. H.; Yoon, S. B.; Yu, J.-S. *J. Mater. Res.* **2003**, *18*, 780.

(11) (a) Kim, J. Y.; Yoon, S. B.; Yu, J.-S. *Chem. Commun*. **2003**, 790. (b) Yoon, S. B.; Sohn, K.; Kim, J. Y.; Chin, C.-H.; Yu, J.-S.; Hyeon, T. *Adv. Mater.* **2002**, *14*, 19. (c) Kim, M. S.; Yoon, S. B.; Sohn, K.; Kim, J. Y.; Chin, C.-H.; Hyeon, T.; Yu, J.-S. *Microporous Mesoporous Mater.* **2003**, *63*, 1.

(12) (a) Watanabe, M.; Uchida, M.; Motoo, S. *J. Electroanal. Chem*. **1987**, *229*, 395. (b) Beden, B.; Kadirgan, F.; Lamy, C.; Leger, J. M. *J. Electroanal. Chem.* **1981**, *127*, 75. (c) Gökagac, G.; Kennedy, B. J.; Cashion, J. D.; Brown, L. J. *J. Chem. Soc., Faraday Trans.* **1993**, *89*, 151. (d) Aricò, A. S.; Kim, H.; Shukla, A. K.; Ravikumar, M. K.; Antonucci, V.; Giordano, N. *Electrochim. Acta* **1994**, *39*, 691. (e) Saffarian, H. M.; Srinivasan, R.; Chu, D.; Gilman, S. *Electrochim. Acta* **1998**, *44*, 1447.

(13) (a) Shukla, A. K.; Ravikumar, M. K.; Aricò, A. S.; Candiano, G.; Antonucci, V.; Giordano, N.; Hamlet, A. *J. Appl. Electrochem.* **1995**, *25*, 528. (b) Shen, P. K.; Tseung, A. C. *J. Electrochem. Soc.* **1994**, *141*, 3082.

(14) (a)Reddington, E.; Sapienza, A.; Gurau, B.; Viswanathan, R.; Sarangpani, S.; Smokin, E. S.; Mallouk, T. E. *Science* **1998**, *280*, 1735. (b) Aricò, A. S.; Poltarzewski, Z.; Kim, H.; Morana, A.; Giordano, N.; Antonucci, V. *J. Power Sources* **1995**, *55*, 159.

(15) (a) Kinoshita, K. *Carbon, Electrochemical, and Physicochemical Properties*; Wiley: New York, 1998. (b) *Carbon Materials for Advanced Technologies*; Burchell, T. D., Ed.; Pergamon: New York, 1999. (c) *Sciences of Carbon Materials*; Marsh, H., Rodrigues-Reinoso, H., Eds.; Publicaciones de la Universidad de Alicante: Alicante, Spain, 1997.

(16) Guerro-Ruiz, A.; Badenes, P.; Rodriguez-Ramos, I. *Appl. Catal. A* **1998**, *173*, 313.

(17) Joo, S. H.; Choi, S. J.; Oh, I.; Kwak, J.; Liu, Z.; Terasaki, O.; Ryoo, R. *Nature* **2001**, *412*, 169.

(18) (a) Bessel, C. A.; Laubernds, K.; Rodriguez, N. M.; Baker, R. T. *J. Phys. Chem. B* **2001**, *105*, 1115. (b) Steigerwalt, E. S.; Deluga, G. A.; Cliffel, D. E.; Lukehart, C. M. *J. Phys. Chem. B* **2001**, *105*, 8097.

(19) Liu, Y. C.; Qiu, X. P.; Huang, Y. Q.; Zhu, W. T.; Wu, G. S. *J. Appl. Electrochem.* **2002**, *32*, 1279.

(20) Yu, J.-S.; Kang, S. K.; Yoon, S. B.; Chai, G. S. *J. Am. Chem. Soc*. **2002**, *124*, 9382.

(21) (a) Osseo-Asare, K.; Arriagada, F. J. *Colloids Surf.* **1990**, *50*, 321. (b) Stober, W.; Fink, A.; Bohn, E. *J. Colloid Inter. Sci.* **1968**, *26*, 62.

(22) (a) Chan, B. C.; Reddington, E.; Sapienza, A.; Yu, J.-S.; Mallouk, T. E.; Gurau, B.; Viswanathan, R.; Liu, R.; Ley, K.; Lafrenz, T. J.; Smokin, E. S.; Sarangapani, S. *Fuel Cells—Clean Energy for Today's World*; 1998, p 1. (b) Reddington, E.; Yu, J.-S.; Sapienza, A.; Chan, B. C.; Gurau, B.; Viswanathan, R.; Liu, R.; Smokin, E. S.; Sarangapani, S.; Mallouk, T. E. *Mater. Res. Soc. Symp. Proc.* **1999**, *549*, 231.

(23) (a) Horvath, G.; Kawazoe, K. *J. Chem. Eng. Jpn*. **1983**, *16*, 470. (b) Valladares, D. L.; Reinoso, F. R.; Zgrablic, G. *Carbon* **1998**, *36*, 1491. (c) Barrett, E. P.; Joyner, L. G.; Halleda, P. P. *J. Am. Chem. Soc.* **1951**, *73*, 373.

(24) (a) Kruk, M.; Jaroniec, M.; Guan, S.; Inagaki, S. *J. Phys. Chem. B* **2001**, *105*, 681. (b) Kruk, M.; Jaroniec, M. *Chem. Mater*. **2001**, *13*, 3169.

(25) Han, S.; Kohn, S.; Hyeon, T. *Chem. Mater*. **2000**, *12*, 3337.

(26) (a) Stonehart, P. *J. Appl. Electrochem.* **1992**, *22*, 995. The minimum surface area that a support material needs to support metal particles was calculated using $SA_{BET} = 6 \times 10^3/Dr_{PtRu}$ equation, where SA_{BET} is a surface area of PtRu metal particles, D is a size of the particles, and r_{PtRu} (density of the particles) = wt % Ptr_{Pt} + wt % Rur_{Ru}. Using the equation and assumption of the PtRu particles as spheres with a 3 nm diameter, a minimum surface area was calculated as 109 m^2 for 1.0 g support in 80 wt % metal loading. (b) Chu, D.; Gilman, S. *J. Electrochem. Soc.* **1996**, *143*, 1685. (c) McCabe, W. L.; Smith, J. C. *Unit operations of chemical engineering*; McGraw-Hill: New York, 2001.

(27) Cullity, B. D. *Elements of X-ray diffraction*; Addison-Wesley Inc.: New York, 1984; Ch. 9.